

Vesicle–Micelle Equilibrium of Anionic and Cationic Surfactant Mixture Studied by Surface Tension

Masumi Villeneuve,^{*,†} Shoji Kaneshina,[‡] Toyoko Imae,[§] and Makoto Aratono[†]

Department of Chemistry, Faculty of Science, Kyushu University 33, Fukuoka 812-8581, Japan, Department of Biological Science & Technology, Faculty of Engineering, The University of Tokushima, Minamijosanjima, Tokushima 770-8506, Japan, and Department of Chemistry, Faculty of Science, Nagoya University, Nagoya 464, Japan

Received July 23, 1998. In Final Form: December 15, 1998

The phase behavior of a very dilute aqueous solution of a sodium decyl sulfate (SDeS)–decyltrimethylammonium bromide (DeTAB) mixture was investigated by the surface tension measurement and partly by the density measurement. The surface tension γ and density ρ were measured as functions of total molality of surfactants \hat{m} and composition of DeTAB \hat{X}_2 . Break points were observed on the curves and identified as the critical vesicle concentration and the concentrations of the initial and final points of the vesicle–micelle coexisting region, respectively. These break points were plotted against \hat{X}_2 , analyzed thermodynamically, and then compared with the ones in the diagrams predicted from a simple model. The composition of DeTAB in the vesicles at the critical vesicle concentration (cvc) was obtained from the cvc versus \hat{X}_2 curve, and it was found out to be 0.5 at almost all \hat{X}_2 values. From the other break point versus \hat{X}_2 plots, the composition region of the vesicle–micelle coexistence in the phase diagram was suggested to be from 0.62 to 0.65. Furthermore, vesicle formation was clearly indicated to take place even at $\hat{X}_2 = 0.9999$, and therefore, the vesicle–micelle transition on the critical aggregation concentration \hat{C} versus \hat{X}_2 curve was expected to sit between $\hat{X}_2 = 0.9999$ and 1.

Introduction

In the recent studies on surfactant solutions, vesicles in some systems have been clarified to be one of the spontaneously formed aggregates. They have been found in many kinds of amphiphile solutions, such as a mixture of single-chain cationic and anionic surfactants,^{1–6} a mixture of a double-chain dimethylammonium surfactant and sodium dodecyl sulfate,⁷ a solution of a double-chain dimethylammonium surfactant with bromide counterion partly exchanged by hydroxide or acetate ion,⁸ a mixture of double-chain dimethylammonium bromide, an *n*-alcohol, and a single-chain ionic surfactant,⁹ mixtures of long-chain lecithin with short-chain lecithin,¹⁰ a solution of a

dimeric surfactant such as alkanediyl- α,ω -bis(dimethyl-dodecylammonium bromide) with an appropriate length of alkanediyl spacer,¹¹ and a solution of a certain kind of glycolipid.¹² The equilibrium between vesicles and micelles or the transition of vesicle to micelle is also intensively studied these days.^{13–17}

Among these systems, aqueous solutions of cationic and anionic surfactant mixtures have been examined in a wide extent of concentrations, and the vesicles formed in such systems have been characterized by Kaler et al.^{1–5} In the ternary phase diagram called the Gibbs triangle at constant temperature and pressure, there are one or two lobes of vesicle solution and several other liquid crystal regions besides that of the micellar solution, depending on the length of the hydrophobic chains, the size of the polar head groups, and the counterions. The vesicle formed in this type of mixture is claimed to be an equilibrium aggregate because of the following three observations according to the criteria of Kaler et al.: (i) vesicles are spontaneously formed when dry surfactant is dispersed into water without mechanical or chemical perturbation; (ii) vesicles do not aggregate with time; and (iii) the vesicle-forming process is reversible.

In spite of the extensive studies on such mixtures, however, the phase diagram has not yet been fully understood, especially in the vicinity of the water corner of the triangle. Therefore, it is important to examine the

* Address for correspondence: Masumi Villeneuve, Department of Biological Science & Technology, Faculty of Engineering, The University of Tokushima, Minamijosanjima, Tokushima 770-8506, Japan. Telephone: 81-886-56-7513. Fax: 81-886-55-3162. E-mail: ville@bio.tokushima-u.ac.jp.

[†] Kyushu University.

[‡] The University of Tokushima.

[§] Nagoya University.

(1) Kaler, E. W.; Herrington, K. L.; Murthy, A. K.; Zasadzinski, J. A. N. *J. Phys. Chem.* **1992**, *96*, 6698.

(2) Kaler, E. W.; Herrington, K. L.; Miller, D. D.; Zasadzinski, J. A. N. In *Phase Behavior of Anionic and Cationic Surfactants Along a Dilution Path: Structure and Dynamics of Strongly Interacting Colloids and Supramolecular Aggregates in Solution*; Chen, S. H.; Huang, J. S.; Tartaglia, P., Eds.; Kluwer Academic Publishers: Dordrecht, The Netherlands, 1992; p 571.

(3) Herrington, K. L.; Kaler, E. W.; Miller, D. D.; Zasadzinski, J. A. N.; Chiruvolu, S. *J. Phys. Chem.* **1993**, *97*, 13792.

(4) Yateilla, M. T.; Herrington, K. L.; Brasher, L. L.; Kaler, E. W.; Chiruvolu, S.; Zasadzinski, J. A. N. *J. Phys. Chem.* **1996**, *100*, 5874.

(5) Soderman, O.; Herrington, K. L.; Kaler, E. W.; Miller, D. D. *Langmuir* **1997**, *13*, 5531.

(6) (a) Huang, J.-B.; Zhao, G.-X. *Colloid Polym. Sci.* **1995**, *273*, 156, (b) Zhao, G.-X.; Yu, W.-L. *J. Colloid Interface Sci.* **1995**, *173*, 159.

(7) Marques, E.; Khan, A.; Miguel, M. G.; Lindman, B. *J. Phys. Chem.* **1993**, *97*, 4729.

(8) Talmon, Y.; Evans, D. F.; Ninham, B. W. *Science* **1983**, *221*, 1047.

(9) Hoffmann, H.; Thunig, C.; Schmiedel, P.; Munkert, U. *Langmuir* **1994**, *10*, 3972.

(10) Gabriel, N. E.; Roberts, M. F. *Biochemistry* **1984**, *23*, 4012.

(11) Danino, D.; Talmon, Y.; Zana, R. *J. Colloid Interface Sci.* **1997**, *185*, 84.

(12) Cantu, L.; Corti, M.; Acquotti, D.; Sonnino, S. *J. Phys. IV* **1993**, *57*.

(13) Salkar, R. A.; Hassan, P. A.; Samant, S. D.; Valaulikar, B. S.; Kumar, V. V.; Kern, F.; Candau, S. J.; Manohar, C. *Chem. Commun.* **1996**, *10*, 1223.

(14) Sein, A.; Engberts, J. B. F. N. *Langmuir* **1995**, *11*, 455.

(15) Lin, Z.; Fu, Y.-C. *J. Colloid Interface Sci.* **1996**, *184*, 325.

(16) Radlinska, E. Z.; Ninham, B. W.; Dalbiez, J. P.; Zemb, T. N. *Colloids Surf.* **1990**, *46*, 213.

(17) Horbaschek, K.; Hoffmann, H.; Thunig, C. *J. Colloid Interface Sci.* **1998**, *206*, 439.

phase behavior in such an extremely dilute region to understand the mechanism of vesicle formation. In our latest study on the mixture of anionic and cationic surfactants, the change of surface tension at concentrations higher than the critical aggregation concentration is carefully observed in order to clarify the aggregation behavior of the surfactants.

Simple experiments of measuring the surface tension of an aqueous solution of surfactant mixtures give some views of aggregation such as aggregation number and micellization degree and even the change in form of the structure of the aggregates. It is a well-known fact that the surface tension decreases as the monomer concentration increases and that it takes a nearly constant value above the critical micelle concentration (cmc). However, the surface tension measured with high accuracy at concentrations above the cmc may predict the aggregation number and change of the composition of the micelle in the case of a mixed surfactant system. In this paper, the term critical aggregation concentration (cac) is introduced to include both critical micelle and critical vesicle concentrations.

Thus, the aqueous solution of a mixture of sodium decyl sulfate (SDeS) and decyltrimethylammonium bromide (DeTAB) was studied by surface tension measurement and partly by density measurement with the aim to clarify the aggregation behavior in the very dilute concentration range. This system is chosen because the monomer solution and the adsorbed film of these surfactant mixtures have been studied in detail by our co-workers.¹⁸ A part of their data was utilized with permission in this study. More than one break point was observed on the surface tension and density versus total molality of surfactants curves at constant composition of DeTAB. It was shown that these break points play a very significant role in constructing phase diagrams of aggregate formation, and even a trace amount of SDeS in the DeTAB aqueous solution turns the micelle solution into the vesicle solution. By applying the thermodynamic relations developed for the vesicle-containing system to the experimental data, we calculated the composition of DeTAB in the vesicle and obtained the phase diagram.

Simple Model of the Concentration–Composition Diagram of Aggregate Formation

Micelles and vesicles never exist separately from the solution, and therefore, they are not phases in the thermodynamic sense. However, we have shown for many cases that our thermodynamic theory of micelle formation,^{19,20} in which micelle particles are treated as if they are macroscopic ones when their thermodynamic quantities are defined in terms of excess ones, is successful in understanding their formation and properties in solution. Here we show a very simple way to predict the coexisting regions of vesicles and micelles in the total molality versus composition diagram which is demonstrated as Figure 1 by using the theory and the mass balance equation.

\hat{C} versus \hat{X}_2 Curve. We suppose that the system contains two ionic surfactants without common ions and that each pure surfactant does not form vesicles but the mixture of them does in a limited composition range. This is the case for the SDeS and DeTAB mixture, and the strong electrostatic molecular interaction between the two

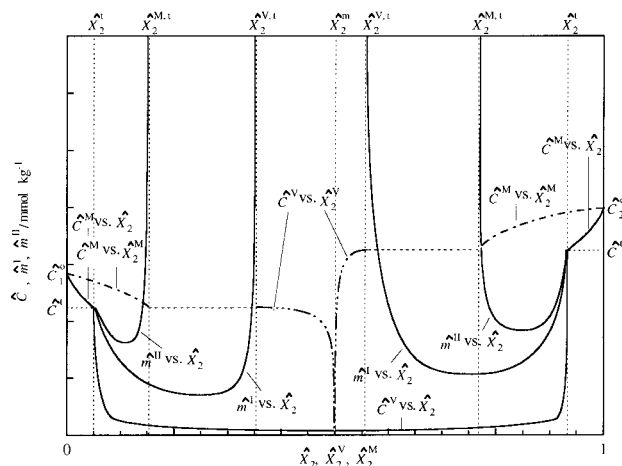


Figure 1. Concentration–composition diagram predicted: (\hat{C}^M vs \hat{X}_2) cmc versus bulk composition curves; (\hat{C}^V vs \hat{X}_2) cvc versus bulk composition curve; (\hat{C}^M vs \hat{X}_2^M) cmc versus composition in the micelle curves; (\hat{C}^V vs \hat{X}_2^V) cvc versus composition in the vesicle curve; (\hat{m}^I vs \hat{X}_2) \hat{m}^I is the total molality where the micelle starts to form in the vesicle solution; (\hat{m}^{II} vs \hat{X}_2) \hat{m}^{II} is the total molality where the vesicle disappears from the vesicle–micelle coexisting solution.

surfactant ions results in a kind of synergism; the concentration of aggregate formation \hat{C} is decreased steeply from their respective pure cmc values by adding the other component.¹⁸ An example of such \hat{C} versus \hat{X}_2 behavior is illustrated by the three curves connected at break points at certain total molalities of \hat{C} and at certain bulk compositions of \hat{X}_2 where the vesicle–micelle transition is assumed to take place in Figure 1. Here, \hat{C}_1^0 and \hat{C}_2^0 are the cmc's of the respective pure surfactants.

\hat{C}^V versus \hat{X}_2^V and \hat{C}^M versus \hat{X}_2^M Curves. The micelle composition \hat{X}_2^M is evaluated by applying

$$\hat{X}_2^M = \hat{X}_2 - (\hat{X}_1\hat{X}_2/\hat{C}^M)(\partial\hat{C}^M/\partial\hat{X}_2)_{T,p} \quad (1)$$

to the critical micelle concentration \hat{C}^M versus \hat{X}_2 curves,^{19,20} and the vesicle composition \hat{X}_2^V is evaluated by applying

$$\hat{X}_2^V = \hat{X}_2 - (\hat{X}_1\hat{X}_2/\hat{C}^V)(\partial\hat{C}^V/\partial\hat{X}_2)_{T,p} \quad (2)$$

to the critical vesicle concentration (cvc) \hat{C}^V versus \hat{X}_2 curves, as will be shown later. Then we have \hat{C}^M versus \hat{X}_2^M and \hat{C}^V versus \hat{X}_2^V schematically given in Figure 1 by heavy dashed lines. Here, $\hat{X}_2^{M,t}$ and $\hat{X}_2^{V,t}$ are the micelle and vesicle compositions at the vesicle–micelle transition point, respectively.

\hat{m}^I versus \hat{X}_2 and \hat{m}^{II} versus \hat{X}_2 Curves. By employing the micelle and vesicle compositions in equilibrium with each other, the mass balance relation of surfactant 2 is given by

$$\hat{m}\hat{X}_2 = \hat{C}^V\hat{X}_2^t + \hat{m}^M\hat{X}_2^{M,t} + \hat{m}^V\hat{X}_2^{V,t} \quad (3)$$

and that of the total surfactants is given by

$$\hat{m} = \hat{C}^V + \hat{m}^M + \hat{m}^V \quad (4)$$

for the vesicle–micelle coexisting region. In these equations it is assumed that the monomer concentration is equal to \hat{C}^V at the given \hat{X}_2 and that the vesicle and micelle compositions are equal to $\hat{X}_2^{V,t}$ and $\hat{X}_2^{M,t}$, respectively, and that they do not change as the total concentration is further increased because vesicle and micelle are regarded as a

(18) Matsuki, H.; Aratono, M.; Kaneshina, S.; Motomura, K. *J. Colloid Interface Sci.* **1997**, *191*, 120.

(19) Motomura, K.; Aratono, M. In *Mixed Surfactant Systems*; Ogino, K., Abe, M., Eds.; Dekker: New York, 1993; p 99.

(20) Motomura, K.; Yamanaka, M.; Aratono, M. *Colloid Polym. Sci.* **1984**, *262*, 948.

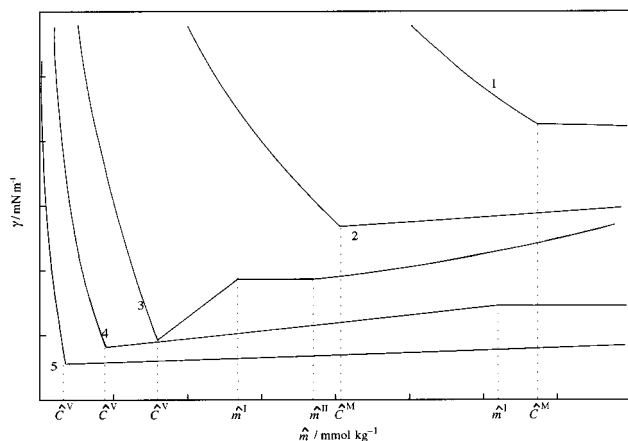


Figure 2. Surface tension versus concentration curves predicted: (1) $\hat{X}_2 = 1$; (2) $\hat{X}_2^m < \hat{X}_2^{V,t} < \hat{X}_2^{M,t} < \hat{X}_2^t < \hat{X}_2 < 1$; (3) $\hat{X}_2^{M,t} < \hat{X}_2^{V,t} < \hat{X}_2^m < \hat{X}_2 < \hat{X}_2^t < 1$; (4) $\hat{X}_2^m < \hat{X}_2^{V,t} < \hat{X}_2 < \hat{X}_2^{M,t} < \hat{X}_2^t < 1$; (5) $\hat{X}_2^m < \hat{X}_2 < \hat{X}_2^{V,t} < \hat{X}_2^{M,t} < \hat{X}_2^t < 1$.

kind of macroscopic phase and they coexist in this regime. First we consider the composition region on the right side of \hat{X}_2^m . At the compositions $\hat{X}_2^{V,t} < \hat{X}_2 < \hat{X}_2^{M,t} < \hat{X}_2^t$, the total concentration \hat{m}^I at which micelle formation starts to take place in the vesicle solution is obtained by putting $\hat{m}^M = 0$ as

$$\hat{m}^I = \hat{C}^V(\hat{X}_2^t - \hat{X}_2^{V,t})/(\hat{X}_2 - \hat{X}_2^{V,t}) \quad (5)$$

At the compositions $\hat{X}_2^{V,t} < \hat{X}_2^{M,t} < \hat{X}_2 < \hat{X}_2^t$, on the other hand, the total concentration \hat{m}^{II} at which vesicle disappears is obtained by putting $\hat{m}^V = 0$ as

$$\hat{m}^{II} = \hat{C}^V(\hat{X}_2^t - \hat{X}_2^{M,t})/(\hat{X}_2 - \hat{X}_2^{M,t}) \quad (6)$$

Therefore, the concentrations \hat{m}^I and \hat{m}^{II} are calculated from the phase diagram of micelle and vesicle formation. In other words, the \hat{m}^I versus \hat{X}_2 and \hat{m}^{II} versus \hat{X}_2 curves are predictable once the values of \hat{X}_2^t , $\hat{X}_2^{V,t}$, and $\hat{X}_2^{M,t}$ are experimentally obtained. It should be noted that vesicle formation takes place in preference to micelle formation in the vesicle–micelle coexisting regions because the relation

$$\hat{m}^I - \hat{C}^V = \hat{C}^V(\hat{X}_2 - \hat{X}_2)/(\hat{X}_2 - \hat{X}_2^{V,t}) > 0 \quad (7)$$

holds at the composition $\hat{X}_2^{V,t} < \hat{X}_2 < \hat{X}_2^t$. Equations 5–7 hold also in the composition region of the left side of \hat{X}_2^m . An example of the \hat{m}^I and \hat{m}^{II} curves is schematically drawn in Figure 1.

Prediction of γ versus \hat{m} Curves. Now the change of surface tension with total concentration can be predicted qualitatively according to the diagram given in Figure 1. This is shown schematically with respect to the right side of \hat{X}_2^m in Figure 2. Curve 1 corresponds to that of the pure surfactant $\hat{X}_2 = 1$: it has one break point on the curve at the cmc, and the surface tension is practically constant at concentrations above the cmc. Curve 2 is the one at the composition $\hat{X}_2 < \hat{X}_2 < 1$: it has one break at the cmc of the surfactant mixture, and the surface tension increases with concentration due to the change of the micelle and monomer compositions. On curve 3 of the compositions $\hat{X}_2^{M,t} < \hat{X}_2 < \hat{X}_2^t$, there exist three break points at \hat{C}^V , \hat{m}^I , and \hat{m}^{II} . It should be noted that the surface tension at concentrations between \hat{m}^I and \hat{m}^{II} is constant due to the vesicle–micelle coexistence. The changes of surface ten-

sion before and after the constant surface tension show the changes of vesicle and micelle compositions with the total concentration. Curve 4 corresponds to the one at $\hat{X}_2^{V,t} < \hat{X}_2 < \hat{X}_2^{M,t}$; vesicles and micelles start to coexist at \hat{m}^I , and vesicles never vanish even at high total molality, and therefore, the surface tension is constant at concentrations above \hat{m}^I . Finally, since there exist only vesicles above the cvc in the composition range $\hat{X}_2^m < \hat{X}_2 < \hat{X}_2^{V,t}$, curve 5 has only one break point, corresponding to \hat{C}^V . The curves qualitatively similar to those in Figure 2 are obtained with respect to the left side of \hat{X}_2^m . The diagram predicted by this simple model will be compared with the one obtained from the thermodynamic analysis of the experimental results.

Experimental Section

Materials. Sodium decyl sulfate (for tenside tests: >99%) was purchased from Merck KGaA (Germany) and purified by recrystallization from ethanol four times. Decyltrimethylammonium bromide (guaranteed reagent: >99%) was purchased from Tokyo Kasei Kogyo Co., Ltd. (Japan) and purified by recrystallizing it three times from a mixture of acetone and ethanol (w/w = 7:3). The purity of the surfactants was confirmed by elemental analysis and by comparing the values of the critical micelle concentration (cmc) with those of the literature.^{20–22} In addition, there was no minimum on the surface tension versus concentration curves in the vicinity of cmc. Water used in all the measurements was triply distilled, the second and third stages being done from alkaline permanganate solution. All the sample solutions were prepared by dispersing a mixture of dry surfactants into water, and they were never sonicated.

Surface Tension. The surface tension γ of the aqueous solutions was measured as a function of the total molality of the surfactants \hat{m} and the composition of DeTAB \hat{X}_2 defined by

$$\hat{m} = 2m_1 + 2\hat{m}_2 \quad (8)$$

and

$$\hat{X}_2 = 2m_2/\hat{m} \quad (9)$$

Here the dissociation of ionic surfactants is explicitly taken into account. All the measurements were performed at 298.15 ± 0.01 K under atmospheric pressure by the drop volume technique described previously.²⁴ Temperature was controlled by use of the water thermostat.

The γ value was reproducible within ± 0.05 mN m⁻¹ at most of the compositions in the whole concentration range. At the compositions $0.9990 \leq \hat{X}_2 < 1$ and concentrations lower than a certain \hat{m} , such a good reproducibility of γ was not obtained by this technique: the surface tension increased by approximately 1.0 mN m⁻¹ as the number of droplets detached from the capillary tip increased. For the determination of the surface tension by the drop volume technique, one drop with adsorbed film at the surface has to be detached from the capillary tip. This may change the composition of the solution remaining in the glass syringe when the composition of the adsorbed film is greatly different from that of the solution. Therefore,

(21) Yamanaka, M.; Kaneshina, S. *J. Solution Chem.* **1990**, *19*, 729.

(22) Mysels, K. J.; Kapauan, P. *J. Colloid Interface Sci.* **1961**, *16*, 481.

(23) De Lisi, R.; Ostiguy, C.; Perron, G.; Desnoyer, J. E. *J. Colloid Interface Sci.* **1979**, *71*, 147.

(24) Motomura, K.; Iwanaga, S.; Hayami, Y.; Uryu, S.; Matuura, R. *J. Colloid Interface Sci.* **1981**, *80*, 32.

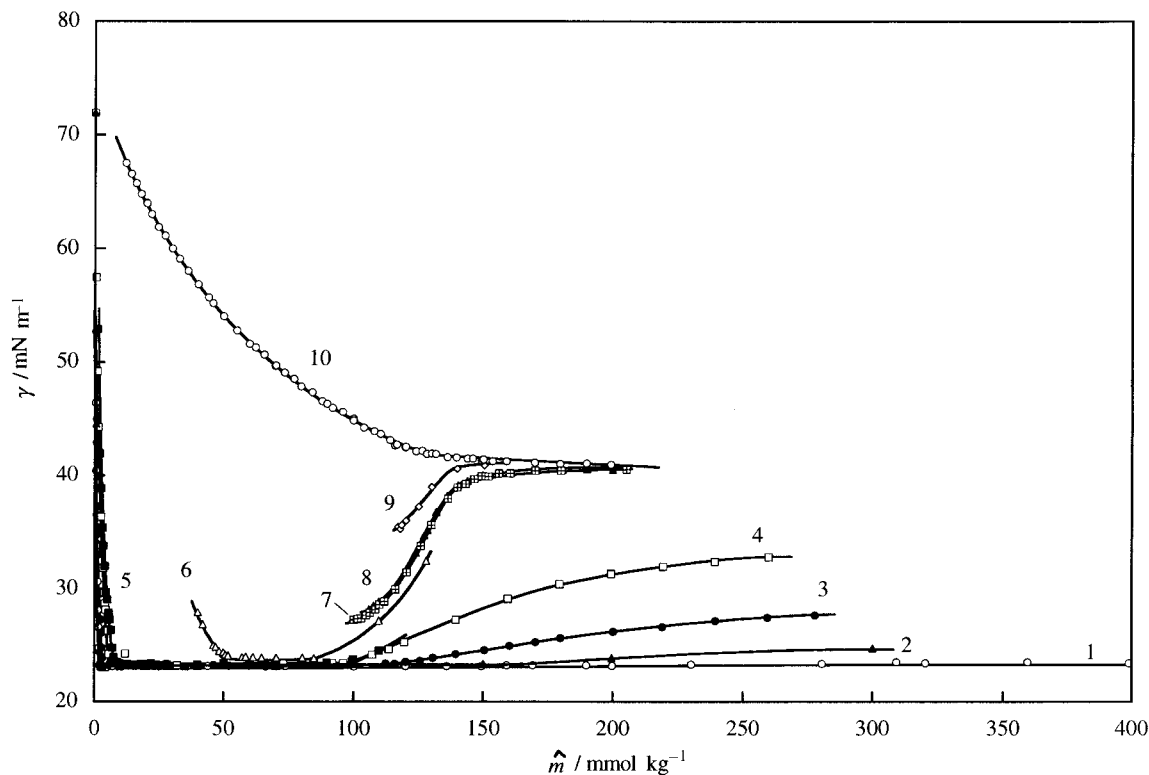


Figure 3. Surface tension versus total molality curves at constant composition: (1) $\hat{X}_2 = 0.7012$; (2) 0.8004; (3) 0.9000; (4) 0.9700; (5) 0.9800; (6) 0.9990; (7) 0.9996; (8) 0.9997; (9) 0.9999; (10) 1.

the above-mentioned phenomenon is easily explained by taking note of the finding that the composition of adsorbed film \hat{X}_2^H is nearly equal to 0.5 at almost all the bulk compositions;¹⁸ the surface adsorption of the minor component SDeS shifts the bulk composition \hat{X}_2 toward 1, and this becomes more influential at higher \hat{X}_2 and lower \hat{m} , where a small shift in bulk composition could change the surface tension greatly. Then, the density of the solution versus total molality curves were employed to determine the cac and the other break points in this particular composition range.

Density. The density of the solutions was measured as a function of \hat{m} and \hat{X}_2 with the vibrating tube densimeter Anton Paar DMA 60/602. The temperature of the measuring cell was maintained at 298.15 ± 0.001 K. Density values were reproducible within ± 0.001 kg m⁻³.

Optical Microscopy. The solutions at $\hat{X}_2 = 0.7012$, 0.9000, and 0.9700 were observed under normal light with a differential interference microscope at 1000 \times magnification (OLYMPUS BX60). The samples were prepared by placing a droplet of the solution in a hole opened in a piece of Teflon rubber sheet pressed between two glass cover slips in order to prevent the solvent from evaporating.

Transmission Electron Microscopy. Samples for the electron microscopy observation (Hitachi electron microscope, H-800) were prepared by freeze-fracture replication (Balzers BAF400). Solutions of the following total molalities and compositions were examined: at $\hat{m} = 2.51$ mmol kg⁻¹, $\hat{X}_2 = 0.7012$; at $\hat{m} = 95.75$ mmol kg⁻¹, $\hat{X}_2 = 0.9999$; and at $\hat{m} = 124.01$ mmol kg⁻¹, $\hat{X}_2 = 0.9999$.

Dynamic Light Scattering. Dynamic light scattering (DLS) was performed on the solutions at $\hat{X}_2 = 0.9999$ and 1 without salt at 298.15 K with an argon laser by MALVERN PS-4700. The samples were transferred into the measurement cell after filtration with a pore size of 0.20 μ m.

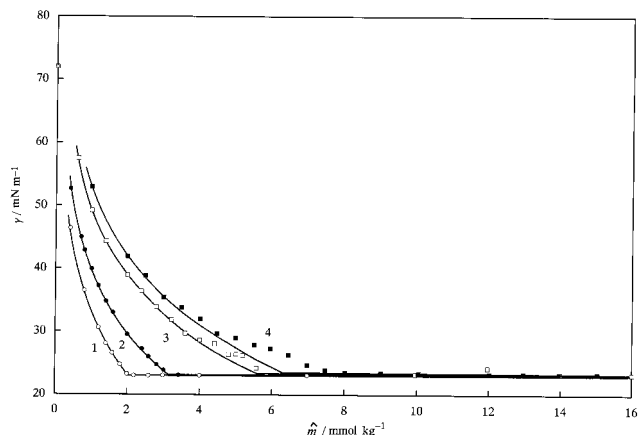


Figure 4. Surface tension versus total molality curves at constant composition: (1) $\hat{X}_2 = 0.7012$; (2) 0.9000; (3) 0.9700; (4) 0.9800.

Results and Discussions

Vesicle Formation of SDeS–DeTAB Mixture. Figure 3 shows the γ versus \hat{m} curves at $\hat{X}_2 = 0.7012$, 0.8004, 0.9000, 0.9700, 0.9800, 0.9990, 0.9996, 0.9997, 0.9999, and 1; the variation of γ with the total molality and composition seems to be different from that of a mixed micelle system. In Figure 4, the curves at $\hat{X}_2 = 0.7012$, 0.9000, 0.9700, and 0.9800 are magnified at the low-concentration ranges. It is seen that γ decreases rapidly as \hat{m} increases and is almost constant above a break point within this concentration range. The shape of the curves looks like that of a usual surfactant mixture, and the solution at \hat{m} a little higher than the break point appears clear and colorless. However, the DLS measurement showed results suggesting the existence of much larger aggregates than micelle particles with the average radius of approximately 500 nm, and furthermore, the vesicles were observed at some values of \hat{X}_2 with the optical

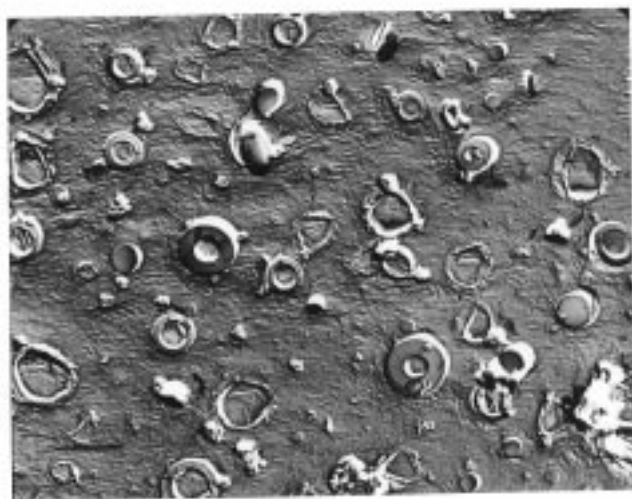
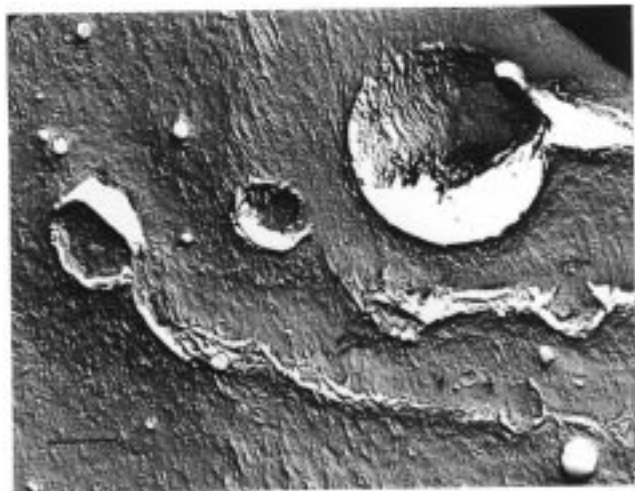


Figure 5. Transmission electron micrographs of a freeze–fracture replica of $\hat{m} = 2.51 \text{ mmol kg}^{-1}$ at $\hat{X}_2 = 0.7012$. Bar = 1000 nm.

microscope. Figure 5 is a TEM image of a freeze–fracture replica of $\hat{m} = 2.51 \text{ mmol kg}^{-1}$, at $\hat{X}_2 = 0.7012$; vesicles with radius ranging from a few hundred nanometers to a few micrometers are seen. Therefore, it is concluded that the break points on these γ versus \hat{m} curves in Figure 4 are referred to as the cvc.

Now, let us look closely at the curves in Figure 3. Figure 6 shows the γ versus \hat{m} curve at $\hat{X}_2 = 0.7012$. Region 1 corresponds to the monomer solution, and the surface tension decreases steeply within a very narrow concentration range. Region 2 starts at $\hat{m} = 2.02 \text{ mmol kg}^{-1}$ and ends at $\hat{m} = 300 \text{ mmol kg}^{-1}$, where γ increases slightly but definitely with the molality. With respect to this increase of γ , we have shown already that the change of surface tension with the total molality above the cmc is related to the changes in the compositions of the mixed micelles and the monomeric solution and is explained by using the surface tension at the cmc versus bulk and micelle compositions diagram.^{25–27}

At the concentrations $2.52 \leq \hat{m} \leq 16.00 \text{ mmol kg}^{-1}$, we observed white powdery precipitates formed within a few

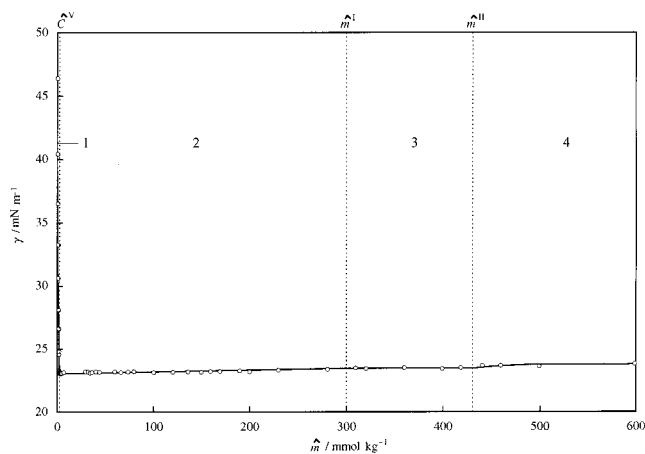


Figure 6. Surface tension versus total molality curve at $\hat{X}_2 = 0.7012$: (1) monomer; (2) monomer + vesicle; (3) monomer + vesicle + micelle coexisting regions.

ten minutes after diluting the stock solution of $\hat{m} = 398.97 \text{ mmol kg}^{-1}$ to these \hat{m} values with water. The solutions were turbid and slightly bluish, although the bluish color disappeared completely by freezing them followed by thawing, and birefringent at some total molalities. It was expected from the turbidity that the aggregates have a size of micrometer order, and in fact, a donut-like shape with a size of a few micrometers was observed by differential interference microscope. In addition, the aggregates formed in the birefringent solution may have lamellar structures because a sheetlike structure was vaguely observed with the differential interference microscope. However, it is seen that the surface tension falls on the same curve despite the change in the structures. Region 3 begins at $\hat{m} = 300.00 \text{ mmol kg}^{-1}$ and ends at $\hat{m} = 446.00 \text{ mmol kg}^{-1}$, where the γ value is constant and the solution is observed to be bluish and transparent. It should be pointed out that the appearance of the solution and the γ value were not changed by freezing the solution followed by thawing it and that the solution appeared to be bluish and transparent even at the highest total molality. Judging from the appearance of the solution and the fact that vesicles were hardly observed by optical microscopy, the size of vesicles in this region is probably around 100 nm or less.

It is important to note a new observation, which is not found in the ordinary mixed micelle systems that the γ value starts to increase again with the molality at $\hat{m} = 446.00 \text{ mmol kg}^{-1}$. The solutions at total molality higher than $446.00 \text{ mmol kg}^{-1}$ become completely clear and colorless, which suggests the absence of vesicle particles. Therefore, we have four regions in this figure: regions 1–4.

The γ versus \hat{m} curve at $\hat{X}_2 = 0.9700$ is shown in Figure 7. At this composition, the four regions are observed as well as at $\hat{X}_2 = 0.7012$. However, it is important to note that region 3 starts at a lower concentration and it is narrower than that in Figure 6, and furthermore, γ increases more greatly with the molality and seems to approach a certain value in region 4. Now it is informative to describe the appearance of the solution at this \hat{X}_2 . It appeared clear and colorless in region 1, turbid and slightly bluish in region 2, bluish and transparent in region 3, and then completely colorless and clear again in region 4. Similarly to the observation at $\hat{X}_2 = 0.7012$, precipitates were observed at the concentrations $2.40 \leq \hat{m} \leq 6.00 \text{ mmol kg}^{-1}$, although they looked flaky rather than powdery. The reproducibility of surface tension was not very good in this concentration range. The surface tension versus

(25) Ikeda, N.; Shiota, E.; Aratono, M.; Motomura, K. *Bull. Chem. Soc. Jpn.* **1989**, *62*, 410.

(26) Matsuki, H.; Ikeda, N.; Aratono, M.; Kaneshina, S.; Motomura, K. *J. Colloid Interface Sci.* **1992**, *150*, 331.

(27) Matsuki, H.; Ikeda, N.; Aratono, M.; Kaneshina, S.; Motomura, K. *J. Colloid Interface Sci.* **1992**, *154*, 454.

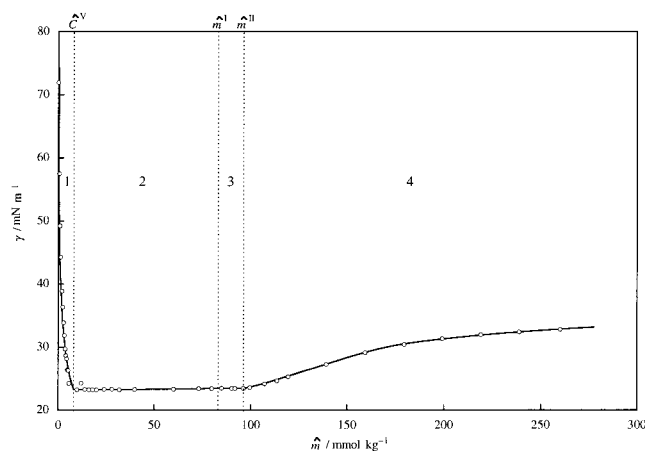


Figure 7. Surface tension versus total molality curve at $\hat{X}_2 = 0.9700$: (1) monomer; (2) monomer + vesicle; (3) monomer + vesicle + micelle; (4) monomer + micelle coexisting regions.

molality curves at $\hat{X}_2 = 0.8004, 0.9000$, and 0.9800 were found to be similar in their shapes to that at $\hat{X}_2 = 0.9700$. Powdery precipitates were also observed at $\hat{X}_2 = 0.9000$ and $1.70 \leq \hat{m} \leq 8.00 \text{ mmol kg}^{-1}$, and flaky ones were observed at $\hat{X}_2 = 0.9800$ and $3.20 \leq \hat{m} \leq 6.00 \text{ mmol kg}^{-1}$.

Now let us compare the surface tension versus concentration plots obtained from the experiments with that from the simple theory in the preceding section. We note that the experimental curve at $\hat{X}_2 = 0.7012$ in Figure 6 and the one at $\hat{X}_2 = 0.9700$ in Figure 7 are similar in qualitative shape to curve 3 in Figure 2. In addition, region 3, where γ takes absolutely constant values, becomes larger as \hat{X}_2 approaches 0.5000. Therefore the regions defined in Figures 6 and 7 are identified as follows. In region 1, the surfactant monomers are dispersed in the solution and vesicles of the surfactant mixture spontaneously form at the molality \hat{C}^V . In region 2, the vesicles and monomers are dispersed in the solution. The composition of surfactants in the vesicles is different from that in monomeric states, and therefore, the surface tension changes with the concentration even at the fixed \hat{X}_2 . In region 3, when the total concentration is increased up to \hat{m}^I , micelles of the surfactant mixture appear and then the vesicles, micelles, and monomers are dispersed in the solution. Since the experiments show the constant surface tension in this region, it is probable that the aqueous solution system behaves as if it has three kinds of macroscopic phases, that is, monomer solution, vesicle, and micelle phases. The concentration is further increased up to the molality \hat{m}^{II} , vesicle particles disappear, and then the micelle particles and monomers are dispersed in the solution in region 4. The change in surface tension values with concentration shows that the composition of the micelle is changed with the concentration.

Taking note of this fairly good correspondence of the experimental findings to the predicted behavior displayed in Figures 1 and 2, it is highly required to measure the surface tension as a function of concentration at different compositions and then show the usefulness of our thermodynamic investigation based on the phase diagram of aggregate formation. With respect to the solution at $\hat{X}_2 = 0.9990, 0.9996, 0.9997$, and 0.9999 , however, surface tension was measurable with the required reproducibility only above a certain concentration; the closer \hat{X}_2 is to 1, the wider the immeasurable concentration range becomes. The results are given in Figure 8. At $\hat{X}_2 = 0.9990$, γ values were reproducible in a part of region 3 and in region 4, and hence, the concentration \hat{m}^{II} was determined. At $\hat{X}_2 = 0.9996, 0.9997$, and 0.9999 , even region 4 was not

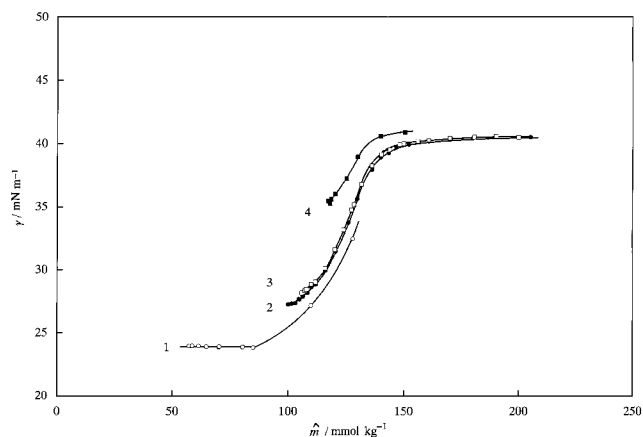


Figure 8. Surface tension versus total molality curves at constant composition: (1) $\hat{X}_2 = 0.9990$; (2) 0.9996 ; (3) 0.9997 ; (4) 0.9999 .

thoroughly measurable. Therefore, we employed the density measurement to determine the concentrations \hat{C}^V , \hat{m}^I , and \hat{m}^{II} at these compositions.

The break points on the density versus total molality curves are shown more clearly on the apparent molar volume ϕ_t versus \hat{m} curve in Figure 9 at $\hat{X}_2 = 0.9997, 0.9999$, and 1. ϕ_t was obtained by

$$\phi_t = 2(1/\rho - 1/\rho_w)/\hat{m} + M/\rho \quad (10)$$

where ρ_w is the density of pure water and M is the mean molar mass of the surfactant mixture defined by

$$M = \hat{X}_2 M_1 + \hat{X}_2 M_2 \quad (11)$$

Here, M_1 and M_2 are the molar masses of SDeS and DeTAB, respectively. The ϕ_t versus \hat{m} curve of the pure DeTAB solution in Figure 9c consists of two curves connected at a break point which is undoubtedly the cmc. Although the ϕ_t versus \hat{m} plots in Figure 9a and b appear to have three break points, the third is actually a bend which corresponds to the one seen around $\hat{m} = 150 \text{ mmol kg}^{-1}$ in Figure 8. The first break point suggests vesicle formation even at $\hat{X}_2 = 0.9999$. By indicating that the values of \hat{m}^I and \hat{m}^{II} become close to each other as \hat{X}_2 approaches \hat{X}_2^* , as shown in Figure 1, the second break may suggest that the \hat{m}^I and \hat{m}^{II} values are located so close to each other that they are indistinguishable at $\hat{X}_2 = 0.9997$ and 0.9999 . Therefore, it is said that regions 1, 2, and 4 were detected by the density measurements at these compositions. This was confirmed by the electron microscopy observation of the solutions of $\hat{m} = 95.75 \text{ mmol kg}^{-1}$ at $\hat{X}_2 = 0.9999$, which is expected to be in region 2, and $\hat{m} = 124.01 \text{ mmol kg}^{-1}$ at $\hat{X}_2 = 0.9999$, which is expected to be in region 4. In Figure 10 of the micrograph of the former solution, almost monodisperse vesicles with diameters of 20–30 nm are observed; they may be unilamellar because some of them were deformed from a sphere in the process of replication and tend to assemble. With respect to the solution of $\hat{m} = 124.01 \text{ mmol kg}^{-1}$ at the same composition, no aggregate was observed, and therefore it is reasonable to conclude that there are no more vesicles at this total molality.

In Figure 11, the concentrations characterizing the vesicle and micelle formations, that is, \hat{C}^V , \hat{m}^I , and \hat{m}^{II} , are plotted against \hat{X}_2 . The diagram very near $\hat{X}_2 = 1$ is magnified in the same figure. Our experiments showed that vesicles are first formed at compositions below $\hat{X}_2 = 0.9999$ and that micelles are first formed at $\hat{X}_2 = 1$ when

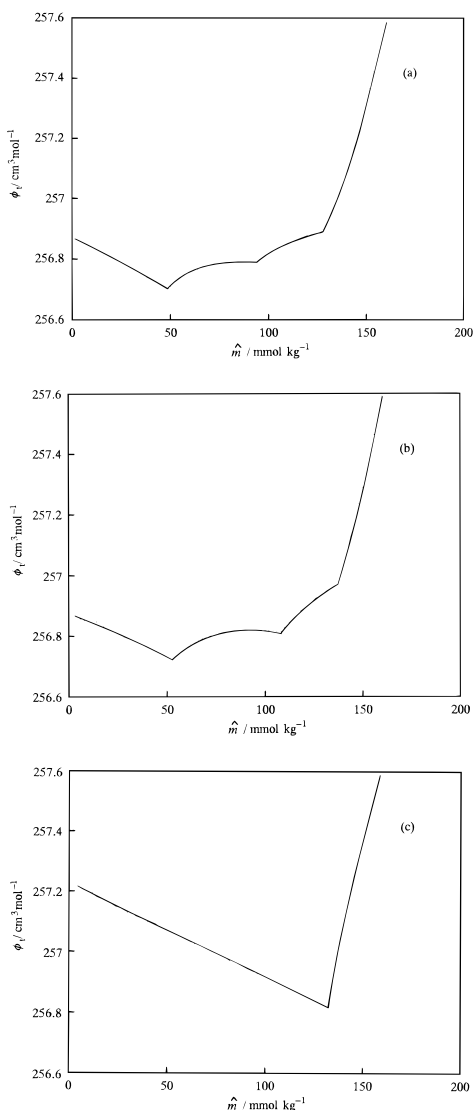


Figure 9. Apparent molar volume versus total molality curve at $\hat{X}_2 =$ (a) 0.9997, (b) 0.9999, and (c) 1.

the total concentration is increased at a given \hat{X}_2 . Therefore, the vesicle–micelle transition is expected to take place at the composition $0.9999 < \hat{X}_2 < 1$, and then the critical aggregation concentration \hat{C} versus \hat{X}_2 curve has a break point between $\hat{X}_2 = 0.9999$ and $\hat{X}_2 = 1$.

Concentration–Composition Diagram of Aggregate Formation. We have shown that the compositions of micelles of a surfactant mixture are evaluated by applying eq 1 to the critical micelle concentration versus bulk composition plot.^{19, 20} We extended the thermodynamic treatment of micelle formation to that of vesicle formation and derived eq 2. Here it should be mentioned that the excess number of each species j , N_j^V , per vesicle particle includes the numbers of the species existing inside the vesicle particle and that the composition of DeTAB and the total number of ions \hat{N}^V in the vesicle are defined by

$$\hat{X}_2^V = (N_{2+}^V + N_{2-}^V) / \hat{N}^V \quad (12)$$

and

$$\hat{N}^V = N_{1+}^V + N_{1-}^V + N_{2+}^V + N_{2-}^V \quad (13)$$

respectively. Hence, the composition in the vesicle \hat{X}_2^V is estimated by applying eq 2 to the \hat{C}^V versus \hat{X}_2 curve in Figure 11.

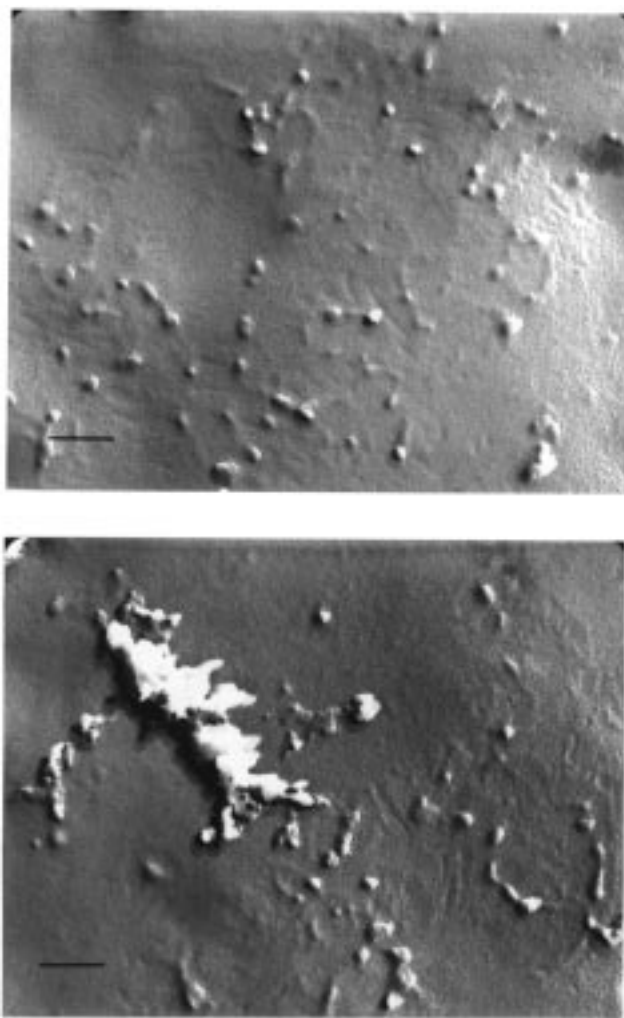


Figure 10. Transmission electron micrographs of $\hat{m} = 95.75$ mmol kg⁻¹ at $\hat{X}_2 = 0.9999$. Bar = 100 nm.

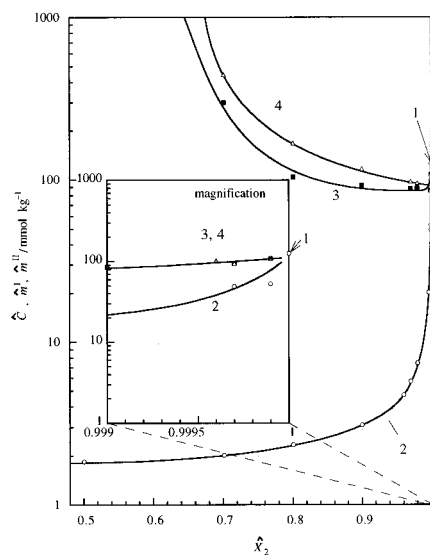


Figure 11. Characteristic concentration versus composition curves: (1) cmc of pure DTAB; (2) \hat{C}^V versus \hat{X}_2 ; (3) \hat{m}^I versus \hat{X}_2 ; (4) \hat{m}^{II} versus \hat{X}_2 .

Figure 12 shows the results of \hat{X}_2^V values in the form of the \hat{C}^V versus \hat{X}_2^V and \hat{X}_2 curves. This is called the phase diagram of vesicle formation. It is found that the \hat{X}_2^V value is close to 0.5 at \hat{C}^V at most of the bulk compositions

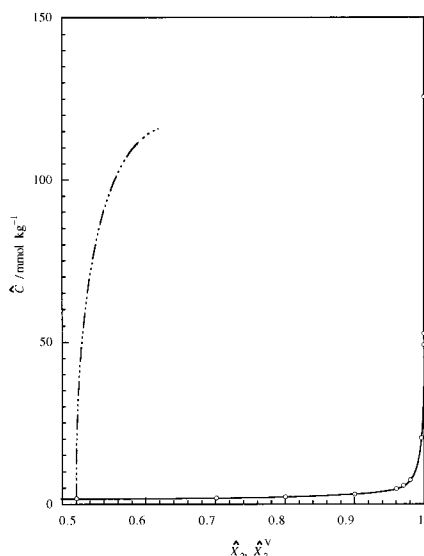


Figure 12. Phase diagram of vesicle formation: (—) \hat{C}^V versus \hat{X}_2 ; (---) \hat{C}^V versus \hat{X}_2^V .

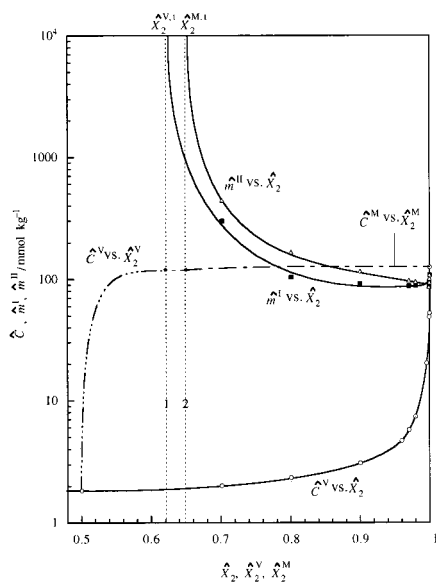


Figure 13. Concentration-Composition diagram: (1) asymptote of the \hat{m}^I versus \hat{X}_2 curve; (2) asymptote of the \hat{m}^{II} versus \hat{X}_2 curve; (—) \hat{C} versus \hat{X}_2 ; (---) \hat{C}^V versus \hat{X}_2^V ; (- · - ·) \hat{C}^M versus \hat{X}_2^M .

investigated. This is a very important result: a vesicle particle contains almost equal numbers of surfactant cations and surfactant anions irrespective of the bulk compositions even when the outside solution of the vesicle contains only 0.01 mol % surfactant anions. The diagram in Figure 12 is again drawn together with \hat{C}^V , \hat{m}^I , and \hat{m}^{II} versus \hat{X}_2 curves in Figure 13. In this figure, the expected curve of \hat{C}^M versus \hat{X}_2^M is also shown, which was not obtained in this study because of the experimental difficulty but is anticipated from the present results. The broken lines denoted by 1 and 2 that are the vertical lines drawn respectively at $\hat{X}_2^{V,t}$ and $\hat{X}_2^{M,t}$ indicate the asymptotes of the \hat{m}^I and \hat{m}^{II} versus \hat{X}_2 curves, which are suggested by the simple model.

According to this diagram, the following changes are expected in the aggregation behavior at different bulk compositions \hat{X}_2 . In the composition range $0.50 < \hat{X}_2 \leq 0.62$, vesicles with $\hat{X}_2^V = 0.5$ are formed at the cvc and the

\hat{X}_2^V value gradually approaches the stoichiometric bulk composition \hat{X}_2 as the total concentration further increases. However, micelle is not formed even at a higher concentration. In the composition range $0.62 < \hat{X}_2 \leq 0.65$, vesicles with $\hat{X}_2^V \approx 0.5$ are formed at the cvc. When the total molality reaches \hat{m}^I , the composition of the vesicle becomes $\hat{X}_2^{V,t}$ and micelles having the composition $\hat{X}_2^{M,t}$ are formed. Further increase in the total concentration changes the fraction of micelle, but vesicle particles never disappear from the solution. In the composition range $0.65 < \hat{X}_2 \leq 0.9999$, vesicles with $\hat{X}_2^V \approx 0.5$ to $\hat{X}_2^{V,t}$ are formed at the cvc. When the total concentration reaches \hat{m}^I , micelle formation begins and the vesicle-micelle coexistence continues until the concentration reaches \hat{m}^{II} . At this \hat{m}^{II} , vesicle disappears and thereafter \hat{X}_2^M changes. In the region between the vesicle-micelle transition point \hat{X}_2^t and $\hat{X}_2 = 1$, micelles are formed at the cmc whose composition is given by the \hat{C}^M versus \hat{X}_2^M curve and then the \hat{X}_2^M value approaches \hat{X}_2 as \hat{m} increases.

Now let us recall that the morphologies of the vesicles are different from each other at $\hat{m} = 2.51 \text{ mmol kg}^{-1}$ and $\hat{X}_2 = 0.7012$ in Figure 5 and at $\hat{m} = 95.75 \text{ mmol kg}^{-1}$ and $\hat{X}_2 = 0.9999$ in Figure 10 and try to find the cause. It is noted here that, at $\hat{X}_2 = 0.7012$, the vesicle size is on the order of micrometers near the cvc and diminishes to the order of 100 nm as the total molality increases to $\hat{m} \approx 300 \text{ mmol kg}^{-1}$. By consulting the phase diagram given in Figure 13, it is said that such a large increase in \hat{m} shifts the composition of vesicle to the cationic surfactant-rich one and results in the decrease of vesicle size. Therefore, the deviation of \hat{X}_2^V from 0.5 to a larger value may be responsible for the smaller radius of the vesicle at $\hat{X}_2 = 0.9999$: the polar head group of DeTAB is larger than that of SDeS, and the excess number of DeTA⁺ surfactant ions over DeS⁻ ions in the outer layer of the bilayer presumably stabilizes the curvature geometrically. Furthermore, the assembly of the spherical vesicles at $\hat{X}_2 = 0.9999$ may be formed due to one of the following two plausible mechanisms: (i) the vesicles are pressed to each other when the solution is frozen in the freeze-fracture process, which is merely an artifact; or (ii) because of the comparatively high concentration of $\hat{m} = 95.75 \text{ mmol kg}^{-1}$, the electric double layer surrounding the vesicle particles may be compressed and, for some reason, the surface charge density of the vesicles is sufficiently low so that they are attracted to each other by the van der Waals attraction.

It is expected that the surface tension versus concentration plots at compositions below $\hat{X}_2 = 0.5$ will give similar shapes to those in Figure 3 because vesicles have never been observed in the pure SDeS solution and the vesicle formation has been reported in the anionic surfactant-rich side in the Gibbs triangles by Kaler et al.^{2,4} Experiments in this composition range are highly required.

Acknowledgment. The authors are very grateful to Mr. T. Iwamoto for taking the freeze-fracture micrographs and to Dr. S. Sasaki for his help with the DLS measurement, and to Dr. M. Matsumoto for the attempt at the cryotransmission electron microscopy experiment. This work was carried out with the support of Grant-in-Aid for Scientific Research (B) No. 10440210 from the Ministry of Education, Science, and Culture of Japan.

LA980925G